Buoyant-Thermocapillary Flow with Nonuniform Supra-Heating: I. Liquid-Phase Behavior

David N. Schiller* and William A. Sirignano†
University of California, Irvine, Irvine, California 92717

A computational study has been made of the transient heat transfer and fluid flow of a circular pool of liquid *n*-decane centrally heated from above by radiation. For the first time, volumetric absorption of the radiation incident on the pool surface is considered. Over the range of gravity levels investigated (0–1 g_n), the flow is primarily thermocapillary-driven. However, buoyancy influences the number and recirculation rates of the subsurface vortices by stabilizing hot subsurface fluid above the colder core fluid. This affects the liquid surface temperature profile which, in turn, governs the velocity profile due to thermocapillarity. For a given heat flux profile from above, the surface temperature and velocity profiles are insensitive to: (a) liquid height for $Re \cdot A^2 >> 1$ (boundary layer flow) and (b) gravity level for $Re \cdot A^2 << 1$ (viscous flow), where A is the aspect ratio of the pool. Volumetric absorption of radiation in the liquid increases the thermal boundary layer thickness, decreases the liquid surface temperature by 20–35%, and increases the temperatures in the core region. However, the velocity field is only slightly changed by the volumetric absorption of radiation.

Nomenclature

A = H'_l/R', aspect ratio of liquid phase
g = $g' t_*/U_*$, gravitational acceleration (≥ 0)
g_n = normal earth gravity (9.81 m/s^2)
H' = height of liquid phase
h = $h'/c_{p*}T_*$, enthalpy
h_1 = $h(T) - h(T = 1)$, excess enthalpy
L_* = characteristic length
P_D = dynamic pressure
q_R = q'_R/q_*, radiative heat flux on liquid surface
q_* = $k_* T_*/L_*$, reference heat flux
R' = radius of cylinder
r = radial coordinate
T = temperature
t = time
U_* = L_*/t_*, reference velocity
u = r-component of velocity
V = velocity vector
v = y-component of velocity
y = axial coordinate
β = volume expansion coefficient
$(\Delta T)_{lg}$ = $T'_{lg}(r = 0) - T'_{lg}(r = 1)$, dimensional
δ_k = δ'_k/L_*, thermal boundary layer thickness
δ_μ = δ'_μ/L_*, momentum boundary layer thickness
σ_T = $\partial\sigma/\partial T$, temperature coefficient of surface tension
σ_o = surface tension at 300 K
σ = Stefan-Boltzmann constant
τ = transmission
ψ = $\psi'/(\rho U L^2)_*$, stream function

Subscripts
h = hot spot (heater)
l = liquid phase
lg = liquid surface
0 = initial condition
$*$ = reference quantity

Superscript
$'$ = dimensional quantity

Standard symbols (ρ, μ, k, etc.) are used for fluid properties. Unless otherwise specified, a variable without a superscript or subscript represents a nondimensional quantity. However, for brevity the primes are omitted in the definition of nondimensional parameters (e.g., Marangoni number). All reference quantities are evaluated at 300 K.

Introduction

VARIATIONS of surface tension due to temperature gradients along a liquid free surface induce thermocapillary (Marangoni) convection. This phenomenon is important in containerless processing,[1] crystal growth,[2,3] welding,[4,5] and flame spread.[6–10] Previous studies of flame spread over liquid fuel pools have shown that when the initial liquid temperature is below the flash point temperature, the rate of flame spread is controlled by convective motions in the liquid ahead of the flame.[11,12] Early experiments[13] attributed the convective motions to buoyancy, but later studies[6,7,11,14] revealed that surface-tension forces dominate. Torrance[8] found that the liquid surface velocity due to thermocapillary convection is of the same order as the flame spread velocity. This suggests that, for liquid fuels at subflash temperatures, parametric studies of liquid behavior without the effects of chemical kinetics may predict accurately trends of flame spread.

The objectives of this two-part paper are to study: (a) the coupling between buoyancy forces and thermocapillary forces in the liquid phase, (b) the effects of gravity level and liquid pool height on the liquid surface temperature and velocity profiles (as these profiles are relevant to ignition delay and flame spread), (c) the effects of variable properties, and (d) the transport of fuel vapor to the heat source. We have introduced the term nonuniform "supra-heating" to describe the nonuniform heating of the liquid surface from above. While the primary application is aimed at ignition delay and flame spread above a liquid fuel pool, the results are also relevant to various crystal growth configurations. The effects of liquid-phase aspect ratio, surface-tension coefficient, and volumetric absorption of radiation will also be investigated in Part I. In Part II, gas-phase coupling, vaporization, and the effects of variable properties will be considered.

Attempts have been made to separate the effects of buoyancy and thermocapillary convection in a liquid with an im-

Received Aug. 3, 1990; revision received Dec. 6, 1990; accepted for publication Dec. 7, 1990.

*Research Assistant. Member AIAA.
†Professor of Mechanical and Aerospace Engineering. Fellow AIAA.

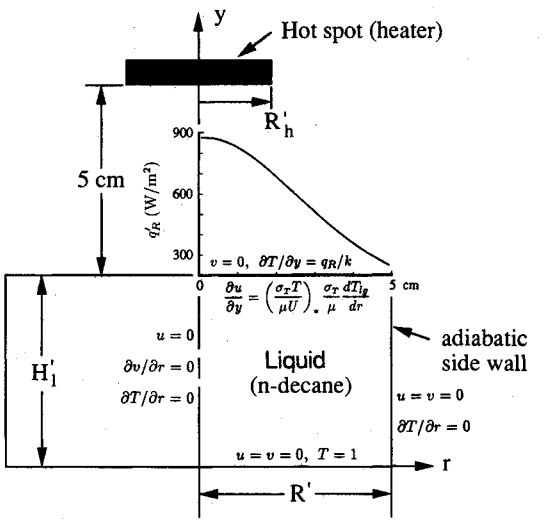

Fig. 1 Geometry of the liquid-only problem, including boundary conditions and plot of radiative heat flux, q'_R, on the liquid surface at $t = 0$ for a 1 cm radius, 800 K heater.

posed temperature difference between two isothermal side walls.[15,16] Metzger and Schwabe[15] varied buoyancy and thermocapillarity experimentally by generating the temperature gradient along the free surface independently from that of the bulk liquid using thermally separated surface and volume heaters along the side walls. They found that buoyancy causes the surface-tension-driven vortex to tend to the surface since this "surface roll" is hotter and, therefore, lighter than the core fluid. The present paper will verify that the primary role of buoyancy with nonuniform supra-heating is the stabilization of warm subsurface fluid above the colder core fluid. It will be shown that, although the subsurface vortex is driven by thermocapillarity rather than by buoyancy, liquid-phase buoyancy and thermocapillarity are coupled. The stable stratification of the liquid pool affects the subsurface isotherms which, in turn, control the surface temperature and velocity profiles (via thermocapillary convection). Metzger and Schwabe[15] also found that for deep pools, the near-surface vortex is almost unchanged in absolute size, extension, and velocity with increasing liquid height. This will be shown to be also true for the case of nonuniform supra-heating as long as $Re \cdot A^2 >> 1$.

The effect of volumetric absorption of radiation on thermocapillary convection has not been assessed in the literature. However, thermocapillary-driven-flows are characterized by thin subsurface boundary layers and, therefore, volumetric absorption of radiation can significantly affect the liquid temperature distribution.

The geometry of the problem is shown in Fig. 1. Here, liquid *n*-decane ($Pr = 12.5$) is contained in an open cylinder of radius R' (5 cm) and height $H' = H'_l$. The initial temperature of the system is uniform at $T' = T'_0 = 300$ K. At $t = 0$, the temperature of a small circular spot (heater) of radius R'_h (1 cm) centrally suspended at a height 5 cm above the liquid increases suddenly to $T' = T'_h$ (800 K or 1000 K) and then remains constant. The radiative heat flux on the liquid surface at $t = 0$ is shown in Fig. 1 for an 800 K heater.

Statement of the Problem

The mathematical formulation of the axisymmetric problem includes variable density and thermophysical properties and a flat and horizontal liquid surface. Unlike most previous studies of thermocapillary convection, the Boussinesq approximation is not made in the present paper. Past studies[17,18] have shown that surface deformation is negligible for small capillary number [for viscous flow, $Ca \equiv A|\sigma_T|(\Delta T)_{lg}/\sigma_o \approx 0.004$ for *n*-decane with $A = 1$ and $(\Delta T)_{lg} = 1°C$]. However, when gravity is important, surface curvature is negligible if the static Bond number, $Bo = \rho g R^2/\sigma_0$, is large. For *n*-decane with $R = 5$ cm, $Bo \approx 760\, g'/g_n$. Refs. 19 and 20 provide a more detailed discussion of the role of free-surface deformation in thermocapillary convection.

The hot spot is assumed black and, unless otherwise specified (see effects of volumetric absorption), the liquid surface is assumed opaque and black. Vaporization and gas-phase conduction and shear stresses are neglected in this Part I paper. They are considered in Part II. Solutocapillary forces are also neglected in both parts of this paper since contamination by surfactants is not applicable.

The nondimensional conservation equations of mass, momentum, and energy follow

$$\frac{\partial \rho}{\partial t} + \frac{1}{r}\frac{\partial}{\partial r}(r\rho u) + \frac{\partial}{\partial y}(\rho v) = 0 \tag{1}$$

$$\frac{\partial(\rho u)}{\partial t} + \frac{1}{r}\frac{\partial}{\partial r}(r\rho u^2) + \frac{\partial}{\partial y}(\rho uv) = - Eu_* \left(\frac{\partial P_D}{\partial r}\right) + \frac{1}{Re_*}\left\{\frac{1}{r}\frac{\partial}{\partial r}\left[r\mu\left(2\frac{\partial u}{\partial r} - \frac{2}{3}\nabla\cdot V\right)\right] + \frac{\partial}{\partial y}\left[\mu\left(\frac{\partial v}{\partial r} + \frac{\partial u}{\partial y}\right)\right] - \frac{\mu}{r}\left(2\frac{u}{r} - \frac{2}{3}\nabla\cdot V\right)\right\} \tag{2}$$

$$\frac{\partial(\rho v)}{\partial t} + \frac{1}{r}\frac{\partial}{\partial r}(r\rho uv) + \frac{\partial}{\partial y}(\rho v^2) = - Eu_* \left(\frac{\partial P_D}{\partial y}\right) + \frac{1}{Re_*}\left\{\frac{1}{r}\frac{\partial}{\partial r}\left[r\mu\left(\frac{\partial v}{\partial r} + \frac{\partial u}{\partial y}\right)\right] + \frac{\partial}{\partial y}\left[\mu\left(2\frac{\partial v}{\partial y} - \frac{2}{3}\nabla\cdot V\right)\right]\right\} + g(1 - \rho) \tag{3}$$

In the liquid, the total pressure (P') is divided into two parts in the computational model: the dynamic pressure (P'_D) and the hydrostatic pressure ($\rho_* g'_y y' = -\rho_* g' y'$).

$$\frac{\partial(\rho h_1)}{\partial t} + \frac{1}{r}\frac{\partial}{\partial r}\left[r\left(\rho u h_1 - \frac{k/c_p}{Pr_* Re_*}\frac{\partial h_1}{\partial r}\right)\right] + \frac{\partial}{\partial y}\left(\rho v h_1 - \frac{k/c_p}{Pr_* Re_*}\frac{\partial h_1}{\partial y}\right) = \dot{Q}_V \tag{4}$$

where $\dot{Q}_V$ is the volumetric absorption of radiation to be defined later (all results are for $\dot{Q}_V = 0$ unless otherwise specified) and the dimensionless Reynolds, Prandtl, and Euler numbers are: $Re_* = U_* L_* / \nu_*$, $Pr_* = \nu_*/\alpha_*$, and $Eu_* = (\Delta P)_*/\rho_* U_*^2$. Reference parameters are $L_* = R'$, $U_* = 1$ cm/s (typical gas phase velocity from Part II of this paper), and $t_* = L_*/U_*$.

The hydrodynamic and thermal boundary conditions are given in Fig. 1 (note that the left side of the computational domain corresponds to the axis of symmetry of the cylinder). For $\dot{Q}_V = 0$, q_R is given by

$$q_R = k\frac{\partial T}{\partial y} = \sigma F_{l-h}(T'^4_h - T'^4_{lg})/q_* \tag{5a}$$

where F_{l-h} is the shape factor from the liquid to the heater.[21]

Scaling Considerations

Scaling of combined buoyancy-thermocapillary-driven flows is complicated by multiple length scales, recirculation, coupling between buoyancy and surface tension, and various time dependent phenomena. Length scales include the radius and height of the hot spot, the radius and height of the liquid, and both the momentum and thermal boundary layer thick-

nesses. Recirculation affects the boundary layer thicknesses and the coupling between buoyancy and surface tension. Despite these complications, some relationships (or at least trends) may be derived (see Ref. 1 and 22–24 for a more comprehensive discussion).

Thermocapillary and buoyancy-driven flows are characterized by the nondimensional Marangoni and Rayleigh numbers, respectively (all quantities on the right-hand sides of equations are dimensional)

$$Ma = \frac{|\sigma_T|(\Delta T)_{lg} R}{\mu\alpha} \tag{6}$$

$$Ra = \frac{\beta g L_*^3 \Delta T}{\nu\alpha} \tag{7}$$

where $(\Delta T)_{lg} = T'_{lg}(r = 0) - T'_{lg}(r = 1)$ is the temperature difference across the liquid surface. By taking $L_* = R$ and $\Delta T = (\Delta T)_{lg}$ in the Rayleigh number, we can form the dynamic Bond number, a ratio of buoyancy to surface-tension forces

$$Bd = \frac{Ra}{Ma} = \frac{\beta\rho g R^2}{|\sigma_T|} \tag{8}$$

For liquid n-decane with $R = 5$ cm, $Bd = 208.6\, g'/g_n$. This indicates that buoyancy forces should dominate thermocapillary forces for $g' \geq 10^{-2}\, g_n$. Although the dynamic Bond number is widely used in the literature for differentially heated side walls, it is debatable whether it is appropriate for the supra-heating case since: 1) horizontal temperature gradients (which lead to buoyancy) exist over only a small thermal boundary layer thickness so that the characteristic length is much smaller than R, and 2) the liquid surface temperature difference is not necessarily representative of the horizontal temperature differences which exist in the boundary layer immediately below the surface.

When the subsurface flow in the liquid is a boundary layer type ($Re \cdot A^2 >> 1$), the characteristic liquid surface velocity and momentum boundary layer thickness scale as

$$Re = U_{lg} R/\nu \sim (Ma/Pr)^{2/3} \tag{9}$$

$$\delta_\mu = \delta'_\mu/R \sim Re^{-1/2} \tag{10}$$

This follows from a balance of viscous stress and surface-tension gradient at the surface. Also, the surface temperature gradient is assumed to be of order $-(\Delta T)_{lg}/R$ and the velocity gradient, $\partial u/\partial y$, is taken to be of order U_{lg}/δ_μ. There is some arbitrariness in which liquid surface velocity is used in the definition of the Reynolds number (e.g., $U_{lg,\max}$ or $\bar{U}_{lg}$). In this paper, Re will be used to denote the Reynolds number based on the area-weighted average liquid surface velocity, $\overline{Re} = \bar{U}_{lg} R/\nu$. For $Pr >> 1$ fluids, the ratio of thermal to momentum boundary layer thicknesses is[24]

$$\delta_k/\delta_\mu \sim Pr^{-1/2} \tag{11}$$

If the subsurface flow is a viscous type ($Re \cdot A^2 << 1$), one obtains

$$Re \sim \frac{Ma}{Pr} \cdot A \tag{12}$$

In this case, the characteristic length for the velocity gradient is the pool depth.

Flux Marangoni and Reynolds numbers may be defined using a reference heat flux for supra-heating; however, these parameters cannot be equated to the Marangoni and Reynolds numbers in scaling considerations.[22]

Scaling $\partial T/\partial y \approx (T_{lg} - T_0)/\delta_k$, Equation (5a) with $T_{lg}^4/T_h^4 << 1$ gives

$$(\Delta T)_{lg} \approx \frac{\sigma\delta_k}{k} [F_{l-h}(r = 0) - F_{l-h}(r = R)] T_h^4 \tag{13}$$

From the equation for the shape factor

$$F_{l-h}(r = 0) - F_{l-h}(r = R) \approx \frac{3}{4} (R_h/R)^2 \tag{14}$$

Finally, combining Eqs. (9)–(11), (13), and (14), one obtains

$$U_{lg} \approx \left(\frac{3|\sigma_T|\sigma}{\rho k}\right)^{1/2} Pr^{-1/4} (R_h/R) T_h^2 \tag{15}$$

$$(\Delta T)_{lg} \approx 0.806 \left(\frac{\sigma^3\mu^2}{\rho k^3 |\sigma_T|}\right)^{1/4} Pr^{-3/8} R_h^{3/2} R^{-1} T_h^3 \tag{16}$$

These expressions are similar to those obtained by Chan[24] using coordinate stretching, asymptotic limits for large Pr, and an arbitrary heat flux. While these formulas provide useful qualitative information on how U_{lg} and $(\Delta T)_{lg}$ may vary with heater size and temperature, Pr, etc., they fail to provide a quantitatively correct prediction of the surface velocity and temperature difference because δ_k and δ_μ vary with r.

Method of Solution

The numerical method uses the SIMPLE algorithm[25] with the SIMPLEC modification[26] and the hybrid-differencing scheme. The momentum and energy equations are said to converge when their normalized residuals are reduced by 5 orders of magnitude (from initial values of 10^{-3}–10^{0}), typically after only 2 or 3 internal iterations of the algorithm. The pressure correction equation is said to converge when either the pressure correction residual is reduced by one order of magnitude (typically to below approximately 10^{-3}), or the residual decreases by less than 0.1% from one iteration to the next. Experience has indicated that this convergence criterion is acceptable.

For n-decane with $R' = 5$ cm and $U'_{lg} = 1$ mm/s, Eqs. (10) and (11) give $\delta'_k \sim 2$ mm. Thus, previously published results relating to the enclosure problem with nonuniform heating from above[21,27,28] used too coarse a mesh in the axial direction ($\Delta y' = 5/3$ mm or coarser). Figure 2 shows results of a grid dependence study for the axial direction. In the radial direc-

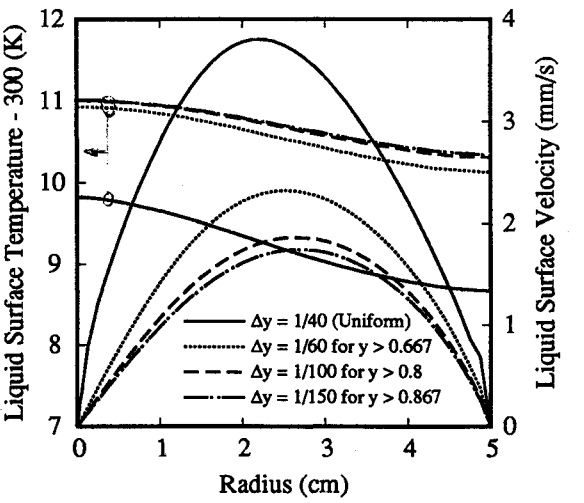

Fig. 2 Effect of grid size below liquid surface on the liquid surface temperature and velocity profiles ($A = 1$, 1 g_n, $t' = 100$ s). A total of 40 cells were used in the axial direction, while 40 uniform cells were used in the radial direction.

tion, 42 grid points (40 uniformly-spaced cells plus 2 columns of boundary node points) were sufficient for a 5-cm radius. An adiabatic side wall condition was assumed to avoid the extremely fine mesh requirements typical of thermocapillary flows with heat loss to a side wall.[29] Results presented in this paper were obtained with a mesh size of ~1/3 mm or less in the axial direction for the first 5 mm below the liquid surface. Unless otherwise specified, a total of 40 cells (42 grid points) were used in the axial direction for a pool depth of 5 cm (less cells were used for shallower pools). A nonuniform mesh with geometric progression was used after the first 5 mm below the liquid surface. The time step was typically 0.025–0.05 s and required approximately 0.26 s of CPU time on a CRAY Y-MP for a 42 × 42 grid.

Results and Discussion

The flow field in the enclosure is presented in terms of the streamlines and the fluid velocities and temperatures. In polar coordinates, the steady-state nondimensional stream function $\psi(r, y)$ is defined by

$$\psi = -\int_0^r \rho r v dr, \qquad \psi = r\int_0^y \rho u dy \tag{17}$$

where $\psi = 0$ at $r = 0, y = 0$. The stream function does not exist for unsteady, variable density flows like the flow studied here; however, for quasi-steady flows, ψ approximately satisfies the continuity equation. Therefore, we employ it for graphical display, but it is not used in the basic analysis to predict the velocity field. Unless otherwise specified, all results will be shown for $t' = 100$ s. At this time, the flow reaches a quasi-steady state, characterized by stabilized boundary layers and vortical structures whose shapes remain essentially constant.

Effects of Gravity Level and Liquid Height

In thermocapillary-driven flow with nonuniform supra-heating, buoyancy stabilizes the hot subsurface fluid above the colder core fluid, thus preventing the thermocapillary-driven vortex from penetrating into the liquid volume. Therefore, the liquid surface temperatures are greater at higher gravity levels. The subsurface isotherms are flatter due to greater radial convection caused by the near-surface recirculation. Since the supra-heating is nonuniform, larger liquid surface temperature gradients and, therefore, larger liquid surface velocities due to Marangoni convection result.

In reduced gravity, the surface fluid recirculates deep into the liquid volume. This leads to colder liquid surface temperatures, since warm fluid which moves radially outward along the surface is replaced by cold fluid from the liquid depths. In contrast to normal gravity, the warm surface fluid is convected downward near the side wall rather than radially inward near the liquid surface. The result of this axial (rather than radial) convection of heat is that at a given height below the liquid surface, the temperature increases with increasing radius; this leads to smaller liquid surface temperature gradients, since the supra-heating is nonuniform, and smaller liquid surface velocities due to Marangoni convection.

Figure 3 illustrates the effect of buoyancy on the subsurface isotherms by comparing temperature profiles at the liquid surface and 1/6 mm below the surface (corresponding to the first interior temperature node of the computational domain) for different gravity levels. Figure 4 shows temperature contours and nondimensional stream function contours for a 1 g_n and a 10^{-4} g_n simulation ($A = 1$). Table 1 summarizes the results of this study for $T_h = 800$ K. Indicated in Table 1 is that, consistent with the decrease of Re, the center of the subsurface vortex (corresponding to the location of $-\psi_{min}$) moves downward and inward with decreasing gravity level for the deeper pools.

As explained above, buoyancy affects the liquid surface temperature and velocity profiles by influencing the vortex structure near the liquid surface. At $t = 0$, surface liquid near the centerline is heated from above and pushed radially outward by thermocapillary forces. The fluid packet continuously gets supra-heated by radiation until it reaches the side wall, at which time it penetrates downward. Buoyancy then dictates how far this fluid will penetrate into the liquid depth. Thus, one would expect that before the time it takes for the fluid packet to travel from the centerline to the side wall, the liquid surface temperature and velocity profiles should be insensitive to gravity level. Figure 5 shows that this is indeed the case.

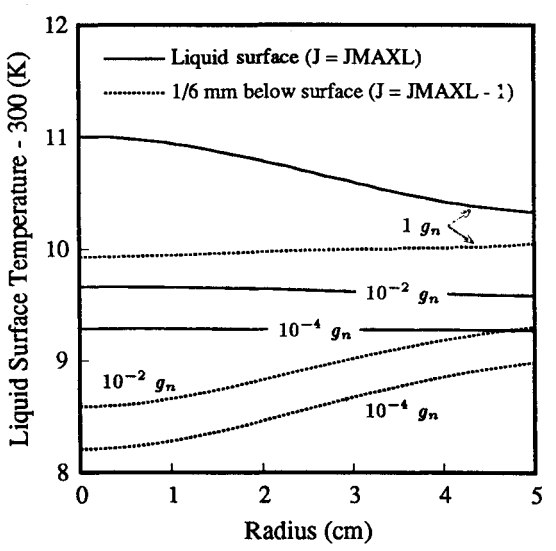

Fig. 3 Temperature profiles at the liquid surface and 1/6 mm below the surface (corresponding to the first interior enthalpy node of the computational domain) for different gravity levels ($A = 1$).

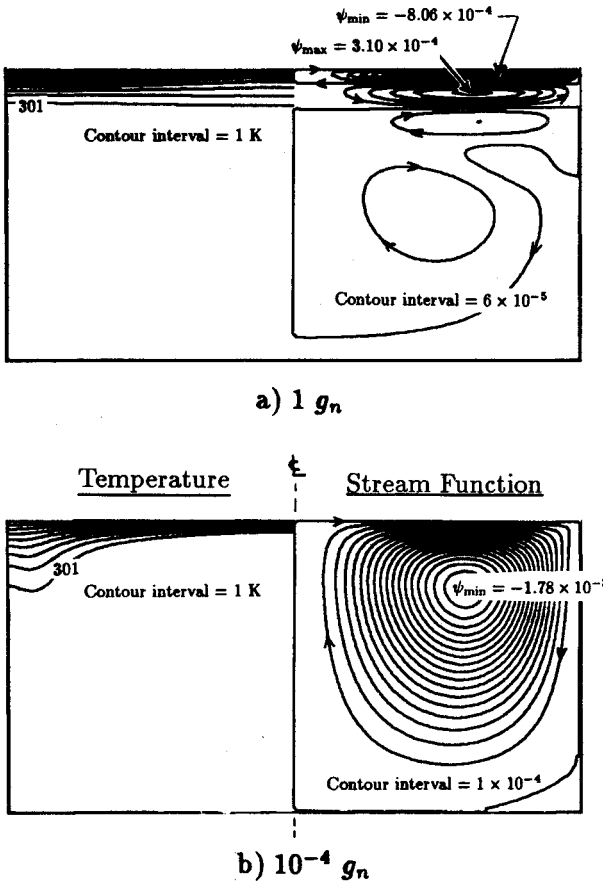

Fig. 4 Temperature contours and nondimensional stream function contours for a 1 g_n and a 10^{-4} g_n simulation ($A = 1$).

Table 1 Summary of results for 800 K heater

g'/g_n	$A = H'/R'$	σ_T	$T'_{lg,max}$ [K]	$(\Delta T)'_{lg}$ [K]	Ma	$U'_{lg,avg}$ [mm/s]	$\overline{Re}$	$\left(\frac{Ma}{Pr}\right)^{2/3}$	ψ_{max}	@ r, y	$-\psi_{min}$	@ r, y
1	1	1	311.01	0.6694	4.59×10^{4}	1.218	56.60	238.0	3.10×10^{-4}	0.625, 0.920	8.06×10^{-4}	0.700, 0.980
1	1/4	1	311.02	0.6704	4.60×10^{4}	1.220	56.69	238.4	3.17×10^{-4}	0.625, 0.170	8.07×10^{-4}	0.700, 0.230
1	1/10	1	310.86	0.6708	4.60×10^{4}	1.183	54.97	238.4	1.34×10^{-4}	0.650, 0.027	7.56×10^{-4}	0.700, 0.080
1	1/20	1	308.34	0.8505	5.83×10^{4}	1.351	62.78	279.2	0	0, 0	8.21×10^{-4}	0.675, 0.035
10^{-2}	1	1	309.67	0.0779	5.34×10^{3}	0.350	16.26	56.7	1.12×10^{-3}	0.675, 0.704	5.81×10^{-4}	0.675, 0.953
10^{-2}	1/4	1	309.78	0.0758	5.20×10^{3}	0.339	15.75	55.7	3.05×10^{-5}	0.800, 0.062	5.66×10^{-4}	0.650, 0.203
10^{-2}	1/10	1	310.12	0.1566	1.07×10^{4}	0.507	23.56	90.2	0	0, 0	6.26×10^{-4}	0.675, 0.067
10^{-2}	1/20	1	308.25	0.7463	5.12×10^{4}	1.273	59.15	256.0	0	0, 0	8.26×10^{-4}	0.675, 0.035
10^{-4}	1	1	309.29	0.0151	1.04×10^{3}	0.211	9.80	19.1	1.02×10^{-7}	0.975, 0.121	1.78×10^{-3}	0.600, 0.757
10^{-4}	1/4	1	309.58	0.0364	2.50×10^{3}	0.256	11.90	34.2	0	0, 0	7.59×10^{-4}	0.625, 0.170
10^{-4}	1/10	1	310.10	0.1470	1.01×10^{4}	0.494	22.96	86.8	0	0, 0	6.29×10^{-4}	0.675, 0.067
10^{-4}	1/20	1	308.24	0.7452	5.11×10^{4}	1.272	59.11	255.7	0	0, 0	8.26×10^{-4}	0.675, 0.035
0	1	1	309.28	0.0143	9.83×10^{2}	0.210	9.76	18.4	6.92×10^{-8}	0.975, 0.121	1.82×10^{-3}	0.600, 0.757
10^{-4}	1	0.5	309.32	0.0302	1.04×10^{3}	0.211	9.80	19.1	8.96×10^{-8}	0.975, 0.121	1.76×10^{-3}	0.600, 0.757
10^{-4}	1	0.25	309.36	0.0608	1.04×10^{3}	0.210	9.76	19.1	7.47×10^{-8}	0.975, 0.121	1.74×10^{-3}	0.600, 0.779
10^{-4}	1	0.1	309.48	0.1537	1.05×10^{3}	0.208	9.67	19.2	5.19×10^{-8}	0.975, 0.121	1.70×10^{-3}	0.600, 0.779
10^{-4}	1	0.01	310.59	1.182	8.11×10^{2}	0.180	8.36	16.1	2.89×10^{-8}	0.975, 0.121	1.55×10^{-3}	0.600, 0.779
10^{-2}	1	0.5	309.75	0.1544	5.29×10^{3}	0.347	16.12	56.4	1.08×10^{-3}	0.675, 0.704	5.78×10^{-4}	0.675, 0.953
10^{-2}	1	0.25	309.91	0.3045	5.22×10^{3}	0.342	15.89	55.9	9.96×10^{-4}	0.675, 0.704	5.71×10^{-4}	0.675, 0.953
10^{-2}	1	0.1	310.32	0.7341	5.03×10^{3}	0.331	15.38	54.5	8.32×10^{-4}	0.675, 0.733	5.53×10^{-4}	0.700, 0.953
10^{-2}	1	0.01	313.55	4.627	3.17×10^{3}	0.221	10.27	40.1	4.03×10^{-4}	0.700, 0.733	4.04×10^{-4}	0.725, 0.953
1	1	0.5	311.44	1.191	4.08×10^{4}	1.124	52.23	220.0	2.82×10^{-4}	0.625, 0.920	7.64×10^{-4}	0.700, 0.980
1	1	0.25	312.04	1.955	3.35×10^{4}	0.985	45.77	192.9	2.44×10^{-4}	0.650, 0.913	7.03×10^{-4}	0.700, 0.980
1	1	0.1	312.95	3.200	2.19×10^{4}	0.760	35.32	145.3	1.81×10^{-4}	0.650, 0.913	6.12×10^{-4}	0.725, 0.980
1	1	0.01	314.36	5.282	3.62×10^{3}	0.389	18.08	43.8	1.21×10^{-4}	0.650, 0.893	4.93×10^{-4}	0.725, 0.973
1	1	0	314.64	5.712	0	0.316	14.68	0	1.16×10^{-4}	0.650, 0.893	4.79×10^{-4}	0.725, 0.973
1	1/10	0	314.53	5.753	0	0.302	14.03	0	1.19×10^{-6}	0.875, 0.007	4.51×10^{-4}	0.725, 0,073
1	1/20	0	312.99	7.438	0	0.266	12.36	0	0	0, 0	3.02×10^{-4}	0.750, 0.030
10^{-2}	1	0	317.70	10.64	0	0.07	3.25	0	1.40×10^{-6}	0.85, 0.121	2.60×10^{-4}	0.750, 0.920
10^{-2}	1/10	0	319.96	13.84	0	0.04	1.86	0	0	0, 0	7.94×10^{-5}	0.725, 0.060
10^{-2}	1/20	0	315.60	11.26	0	0.005	0.23	0	0	0, 0	4.69×10^{-6}	0.725, 0.030
10^{-4}	1	0	321.07	15.10	0	0.004	0.19	0	0	0, 0	3.28×10^{-5}	0.625, 0.828
10^{-4}	1/10	0	320.90	15.03	0	0.0006	0.03	0	8.23×10^{-7}	0.625, 0.093	5.15×10^{-7}	0.875, 0.053

Table 2 Summary of results for 1000 K heater

g'/g_n	$A = H'/R'$	σ_T	$T'_{lg,max}$ [K]	$(\Delta T)'_{lg}$ [K]	Ma	$U'_{lg,avg}$ [mm/s]	$\overline{Re}$	$\left(\frac{Ma}{Pr}\right)^{2/3}$	ψ_{max}	@ r, y	$-\psi_{min}$	@ r, y
1	1	1	327.26	0.9797	6.72×10^{4}	1.838	85.41	306.9	3.55×10^{-4}	0.600, 0.631	9.33×10^{-4}	0.700, 0.987
1	1/4	1	327.27	0.9795	6.72×10^{4}	1.838	85.41	306.9	3.22×10^{-4}	0.625, 0.183	9.33×10^{-4}	0.700, 0.237
1	1/10	1	326.93	0.9818	6.73×10^{4}	1.815	84.34	307.2	2.72×10^{-4}	0.625, 0.040	9.12×10^{-4}	0.700, 0.087
10^{-2}	1	1	324.67	0.1327	9.10×10^{3}	0.502	23.33	80.9	2.17×10^{-3}	0.575, 0.631	6.21×10^{-4}	0.675, 0.967
10^{-2}	1/4	1	324.80	0.1204	8.26×10^{3}	0.473	21.98	75.9	2.38×10^{-4}	0.650, 0.093	5.77×10^{-4}	0.675, 0.217
10^{-2}	1/10	1	325.20	0.1528	1.05×10^{4}	0.555	25.79	89.0	0	0, 0	6.07×10^{-4}	0.675, 0.067
10^{-4}	1	1	323.20	0.0151	1.04×10^{3}	0.220	10.22	19.1	2.15×10^{-7}	0.950, 0.121	1.75×10^{-3}	0.600, 0.757
10^{-4}	1/4	1	323.95	0.0344	2.36×10^{3}	0.269	12.50	32.9	0	0, 0	7.42×10^{-4}	0.625, 0.170
10^{-4}	1/10	1	325.13	0.1297	8.89×10^{3}	0.515	23.93	79.7	0	0, 0	6.16×10^{-4}	0.675, 0.067
0	1	1	323.16	0.0132	9.05×10^{2}	0.216	10.04	17.4	9.00×10^{-8}	0.975, 0.121	1.86×10^{-3}	0.600, 0.757
10^{-4}	1	0.1	323.48	0.1509	1.03×10^{3}	0.218	10.13	18.9	1.24×10^{-7}	0.975, 0.121	1.68×10^{-3}	0.575, 0.779
10^{-2}	1	0.1	325.88	1.271	8.72×10^{3}	0.489	22.72	78.7	1.49×10^{-3}	0.575, 0.704	6.01×10^{-4}	0.675, 0.967
1	1	0.1	330.90	5.563	3.81×10^{4}	1.267	58.88	210.2	2.15×10^{-4}	0.600, 0.670	7.29×10^{-4}	0.725, 0.987

Simulations with larger radius cylinders verify that gravity significantly affects the T_{lg} and U_{lg} profiles only after this characteristic time (which, of course, increases with increasing R'). Note that, at all gravity levels and pool heights investigated, the vortical structures became quasi-steady before the subsurface vortex went through one recirculation. The circulation time of the subsurface vortex is given approximately by $t'_{circ} \approx t_* h/|\psi_{min}|$, where h is the nondimensional subsurface vortex height; for example, at 1 g_n($A = 1$): $h \approx 0.05$, $|\psi_{min}| = 8.06 \times 10^{-4} \rightarrow t'_{circ} \approx 310$ seconds.

The surface temperature and velocity profiles are strong functions of the subsurface vortex height. When multiple vortices are formed in the liquid (typically for boundary layer flow, where $Re \cdot A^2 >> 1$), the liquid surface temperature and velocity profiles will be insensitive to H_l as long as H_l is greater than the height of the subsurface vortex. This is consistent with past studies on the effects of pool height on flame spread rates.[8] For example, consider the 1 g_n flow shown in Figure 4. The subsurface vortex height is approximately 2.5 mm, and as can be seen from Runs 1–3 in Table 1, the liquid surface profiles change very little for pool depths of 5 mm or more. In a reduced gravity scenario in which a single vortex fills the liquid volume, decreasing H_l will decrease the subsurface vortex height, thus, making the vortex resemble the subsurface

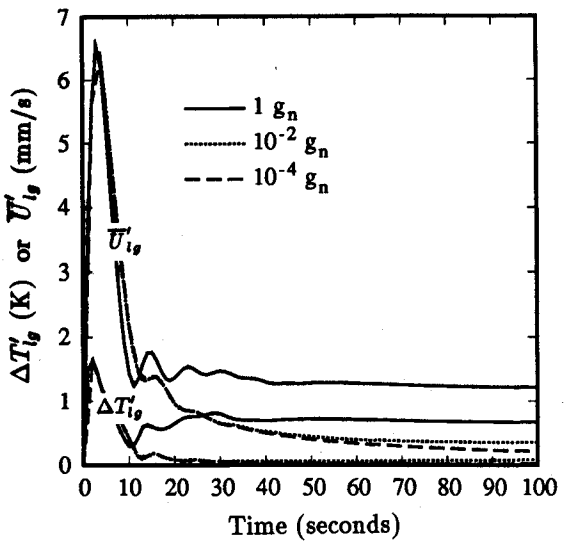

Fig. 5 Liquid surface temperature difference, $\Delta T'_{lg}$, and area-weighted average liquid surface velocity, $\overline{U}'_{lg}$, as a function of time for different gravity levels (A = 1).

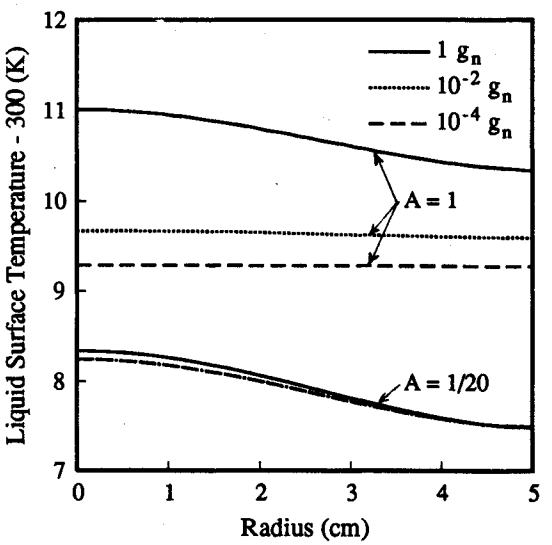

Fig. 6 Liquid surface temperature profiles at different gravity levels for deep (A = 1) and shallow (A = 1/20) pools. A single vortex formed in the liquid at 1 g_n for A = 1/20, at 10^{-2} g_n for A < 1/4, and at 10^{-4} g_n for all aspect ratios investigated.

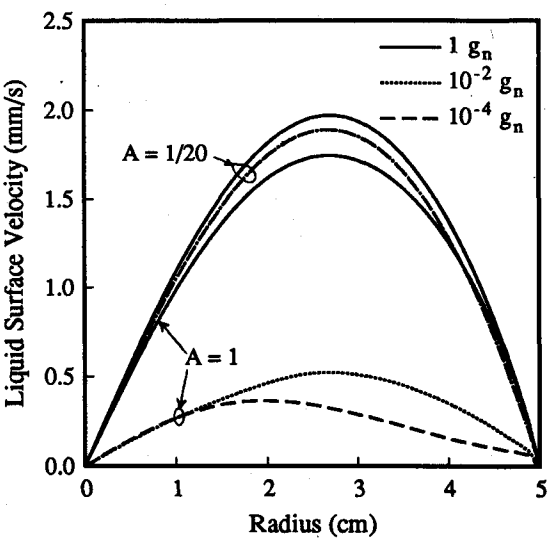

Fig. 7 Liquid surface velocity profiles at different gravity levels for deep (A = 1) and shallow (A = 1/20) pools.

vortex of a higher gravity level simulation. Thus, for shallow pools, in which a single vortex fills the liquid (typically for viscous flow, where $Re \cdot A^2 << 1$), one would predict that the liquid surface temperature and velocity profiles will be insensitive to gravity level. This is seen to be true by examining Figs. 6 and 7, in which the liquid surface temperature and velocity profiles at different gravity levels are compared for deep and shallow pools. Note that a single vortex formed in the liquid at 10^{-2} g_n for $A < 1/4$, and at 10^{-4} g_n for $A \leq 3$.

Ignition delay and flame spread rates are functions of liquid surface temperature and velocity as well as gas phase heat and mass transport. Therefore, one consequence of the above is that, for a given heat flux profile from above, the ignition delay time and flame spread rate will be governed by *gas phase* heat and mass transport: 1) independent of H_l for given g if $\overline{Re} \cdot A^2 >> 1$ (boundary layer flow) and 2) independent of gravity effects in the liquid for given H_l if $\overline{Re} \cdot A^2 << 1$ (viscous flow).

One limitation of the above findings is that the Reynolds and Marangoni numbers are not known *a priori* with nonuniform supra-heating. Thus, for a given liquid surface heat flux distribution and gravity level, one must rely on experience to know whether the flow will be a viscous or boundary layer type. The aforementioned trends are the same for a 1000 K hot spot (see Table 2). As expected, the liquid surface temperatures and velocities increase with increasing heater temperature. Consistent with the increase of liquid surface velocity, the location of $-\psi_{\min}$ is also closer to the surface at higher T_h.

Effects of Varying the Surface-Tension Coefficient

Runs 14–25 in Table 1 show the effect of decreasing the value of the surface-tension coefficient, σ'_T, below its normal value for n-decane [$\sigma'_{T,*} = -9.2 \times 10^{-5}$ N/(m·K)]. Comparing Run 9 with Runs 14–17 in Table 1, we see that decreasing σ_T by two orders of magnitude at 10^{-4} g_n has little effect on the surface velocity and Marangoni number because $(\Delta T)_{lg} \propto \sigma_T^{-1}$ over this range. This was not predicted by Eq. (16), which was obtained by an oversimplified scaling analysis. The same insensitivity of U_{lg} to σ_T is evident at 10^{-2} g_n for $0.1 \leq \sigma_T \leq 1$. Although radial convection of heat due to buoyancy forces has a greater influence on $(\Delta T)_{lg}$ at 1 g_n than at the reduced gravity levels, comparison of Run 1 with Runs 22–24 shows $\overline{Re} \propto (Ma/Pr)^{2/3}$, indicating that the flow is thermocapillary-driven even at 1 g_n.

Effects of Volumetric Absorption of Radiation

The transmissivity of liquid n-decane as a function of depth [$\tau(L')$, Fig. 8] was determined from measurements of the complex index of refraction ($n + i\hat{k}$) using Beer's Law and values of the external fractional function, f_e

$$\tau(L') = \sum_{i=1}^{50} \Delta f_e(\lambda'_i) \exp[-4\pi \hat{k}_i (L'/\lambda'_i)] \qquad (18)$$

where $L' \equiv H' - y'$. The spectral data for λ = 2.5–15 μm was divided into 50 bands for the calculations, with λ'_i and $\hat{k}_i$ being the average wavelength and extinction coefficient over the i^{th} band. Using an average value of $n \approx 1.5$, the reflectivity of n-decane was taken as $(n-1)^2/(n+1)^2 = 0.04$. The radiation transmitted past the phase interface passes downward into the liquid at a small angle θ from the normal. Since $\cos\theta \sim 1$ ($\cos\theta_{\max} = 0.882$), we assume the radiation from the heater penetrates vertically through the liquid at all radii. Using the $\tau(L')$ data, $\dot{Q}_V$ in Eq. (4) is given by

$$\dot{Q}_V = \frac{1}{Re_* Pr_*} \frac{L_*}{q_*} \left(-\frac{\partial \tau}{\partial L'} \right) \sigma F_{l-h} T'^4_h \qquad (19)$$

Note that the approximation $\tau \approx e^{-aL'}$ (where a is a single gray absorption coefficient) was found to be good only for $L' > 4.5$ mm, and, hence, was not used in the calculations.

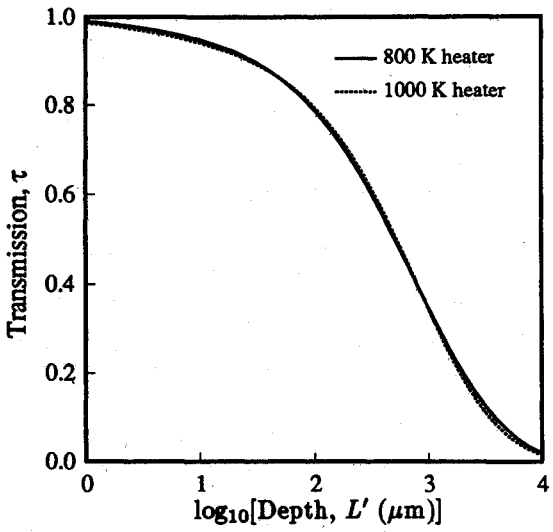

Fig. 8 Transmission of liquid *n*-decane as a function of depth (L') for black-body radiation from an 800 K and 1000 K heater.

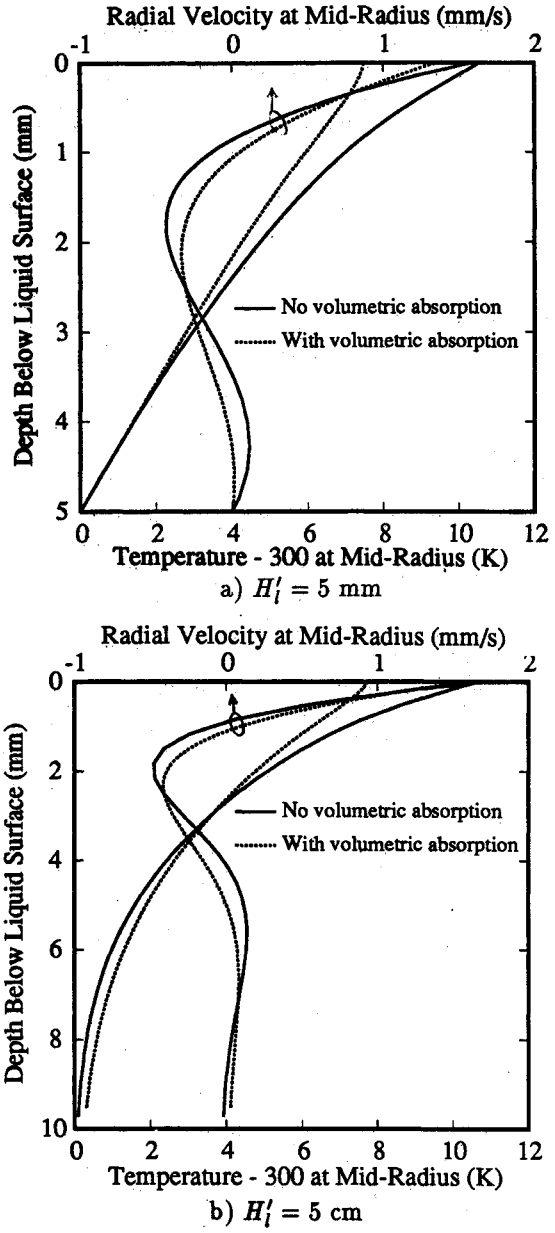

Fig. 9 Temperature and velocity profiles at mid-radius with and without volumetric absorption of radiation for a) shallow and b) deep pools (1 g_n, T_h = 800 K).

Since τ decreases rapidly with depth for $L' < 1$ mm, the grid in the axial direction was refined considerably in order to obtain "grid independent" results (a 50 μm mesh was used for the first 1–2 mm below the liquid surface). Some surface absorption of radiation was incorporated into the liquid surface boundary condition by using

$$q_R = \sigma F_{l-h} T_h'^4 (1 - \tau_{\text{surf}})(1 - \text{reflectivity})/q_* \quad (5b)$$

where τ_{surf} (=0.91) is the transmission at the depth which corresponds to the first interior enthalpy node of the computational domain.

As shown in Fig. 9, volumetric absorption of radiation in the liquid increases the thermal boundary layer thickness, decreases the liquid surface temperature by 20–35%, and increases the temperatures in the core region. However, the velocity field is only slightly changed by the volumetric absorption of radiation. Although the liquid surface temperatures are lower when absorption is considered, the surface temperature gradients are still functions of the shape factor profile, $F_{l-h}(r)$. These temperature gradients drive the flow via thermocapillary convection. The absorption of radiation also alters the core fluid temperatures which contribute to natural convection; however, these effects are negligible compared to thermocapillary convection, even at 1 g_n.

Conclusions

A computational study was made of transient heat transfer and fluid flow of liquid *n*-decane supra-heated nonuniformly in a 5-cm radius axisymmetric cylinder. The liquid surface was assumed flat and horizontal at all gravity levels studied (0–1 g_n), and the side walls were assumed adiabatic. Results show that the subsurface isotherms at 1 g_n are nearly parallel to the liquid surface, and, therefore, the flow is thermocapillary-driven even at 1 g_n, where $Bd = Ra/Ma >> 1$. The magnitude of the dynamic Bond number based upon a global length scale cannot, therefore, be used to reach conclusions about subregions of the field for nonuniform supra-heating.

Buoyancy influences the vortical structure by stabilizing hot subsurface fluid above the colder core fluid. This affects the liquid surface temperature profile, which, in turn, governs the velocity profile via Marangoni convection. Thus, the effects of buoyancy and thermocapillarity are highly coupled for the case of heating from above. The surface temperature and velocity profiles (T_{lg} and U_{lg}) are strong functions of the subsurface vortex height; for a given heat flux profile incident on the liquid surface, T_{lg} and U_{lg} are insensitive to 1) liquid height for $Re \cdot A^2 >> 1$ (boundary layer flow) and 2) gravity level for $Re \cdot A^2 << 1$ (viscous flow). This has important implications to ignition delay and flame spread, which are functions of liquid surface temperature and velocity as well as gas-phase heat and mass transport. Increasing the heater temperature increases the average liquid surface temperature and velocity and (consistent with scaling) decreases the subsurface vortex height.

Decreasing the surface-tension coefficient, σ_T, by one or two orders of magnitude under microgravity conditions had little effect on the Marangoni number and the velocity field because the liquid surface temperature difference, $(\Delta T)_{lg}$, varied inversely to σ_T. At 1 g_n, radial convection of heat due to buoyancy forces has a greater influence on $(\Delta T)_{lg}$ than at the reduced gravity levels, and therefore Ma and U_{lg} decreased with σ_T.

Complex index of refraction data was used to find the transmission of liquid *n*-decane as a function of depth. Approximately two-thirds of the incident radiation from an 800 K or 1000 K heater is absorbed in the first 1 mm of the liquid. However, the subsurface thermal boundary layer thickness is only a few millimeters, and therefore, volumetric absorption significantly alters the temperature field. While volumetric

absorption of radiation in the liquid decreases the liquid surface temperature by 20–35%, the velocity field is only slightly changed because the surface temperature gradients are still functions of the shape factor profile, $F_{l-h}(r)$.

Appendix—Physical Properties

For liquid *n*-decane, the following correlations were used (derived from Refs. 30 and 31):

density [kg/m^3]: $\rho' = 724.42 - 234.785(T - 1.0)$

heat capacity [J/kg·K]: $c_p' = 2214.86 + 1056.42(T - 1.0)$

thermal conductivity [W/m·K]: $k' = 0.1381 - 0.0982(T - 1.0)$

dynamic viscosity [kg/m·s]: $\mu' = 7.794 \times 10^{-4} T^{-5.4009}$

Acknowledgment

Research at the University of California at Irvine was conducted in support of NASA Grant NAG 3-627 under the technical monitoring of H. Ross (NASA-LeRC). The computational research was supported in part by the San Diego Supercomputer Center through an allocation of computer time. We are indebted to Boris Abramzon who wrote the original algorithm of our computer code and several of the subroutines. The authors are grateful to H. Ross for his experimental support and technical discussions, and A. Tuntomo and D. K. Edwards for their assistance in incorporating volumetric absorption of radiation in the numerical model. We would also like to thank Professors M. Chen and T. Bergman for helping explain why this seemingly simple problem involves numerous intricacies.

References

[1]Ostrach, S., "Low-Gravity Fluid Flows," *Annual Review of Fluid Mechanics*, Vol. 14, 1982, pp. 313–345.

[2]Ostrach, S., "Fluid Mechanics in Crystal Growth—The 1982 Freeman Scholar Lecture," *Journal of Fluids Engineering*, Vol. 105, 1983, pp. 5–20.

[3]Schwabe, D., "Marangoni Effects in Crystal Growth Melts," *PhysicoChemical Hydrodynamics*, Vol. 2, No. 4, 1981, pp. 263–280.

[4]Oreper, G. M., and Szekely, J., "Heat- and Fluid-Flow Phenomena in Weld Pools," *Journal of Fluid Mechanics*, Vol. 147, 1984, pp. 53–79.

[5]Ramanan, N., and Korpela, S. A., "Thermocapillary Convection in an Axi-Symmetric Pool," *Computers & Fluids*, Vol. 18, No. 2, 1990, pp. 205–215.

[6]Sirignano, W. A., and Glassman, I., "Flame Spreading Above Liquid Fuels: Surface-Tension-Driven Flows," *Combustion Science and Technology*, Vol. 1, 1970, pp. 307–312.

[7]Mackinven, R., Hansel, J. G., and Glassman, I., "Influence of Laboratory Parameters on Flame Spread Across Liquid Fuels," *Combustion Science and Technology*, Vol. 1, 1970, pp. 293–306.

[8]Torrance, K. E., and Mahajan, R. L., "Fire Spread Over Liquid Fuels: Liquid Phase Parameters," *Fifteenth Symposium on Combustion*, Combustion Institute, Pittsburgh, 1974, pp. 281–287.

[9]Glassman, I., and Dryer, F. L., "Flame Spread Across Liquid Fuels," *Fire Safety Journal*, Vol. 3, 1980/1981, pp. 123–138.

[10]Ito, A., Masuda, D., and Saito, K., "A Study of Flame Spread Over Alcohols Using Holographic Interferometry," Combustion and Flame, Vol. 83, 1991, pp. 375–389.

[11]Glassman, I., and Hansel, J. G., "Some Thoughts and Experiments on Liquid Fuel Spreading, Steady Burning and Ignitability in Quiescent Atmospheres," *Fire Research Abstracts and Reviews*, Vol. 10, 1968, pp. 217–234.

[12]Akita, K., "Some Problems of Flame Spread Along a Liquid Fuel Surface," *Fourteenth Symposium on Combustion*, Combustion Institute, Pittsburgh, 1973, pp. 1075–1083.

[13]Burgoyne, J. H., Roberts, A. F., and Quinton, P. G., "The Spread of Flame Across a Liquid Surface: I. The Induction Period, II. Steady-State Conditions, III. A Theoretical Model," *Proceedings of the Royal Society*, Vol. A308, 1968, pp. 39–79.

[14]Glassman, I., Hansel, J. G., and Eklund, T., "Hydrodynamic Effects in the Flame Spreading, Ignitability and Steady Burning of Liquid Fuels," *Combustion and Flame*, Vol. 13, 1969, pp. 99–101.

[15]Metzger, J., and Schwabe, D., "Coupled Buoyant and Thermocapillary Convection," *PhysicoChemical Hydrodynamics*, Vol. 10, No. 3, 1988, pp. 263–282.

[16]Villers, D., and Platten, J. K., "Separation of Marangoni Convection From Gravitational Convection in Earth Experiments," *PhysicoChemical Hydrodynamics*, Vol. 8, No. 2, 1987, pp. 173–183.

[17]Kamotani, Y., and Ostrach, S., "Design of a Thermocapillary Flow Experiment in Reduced Gravity," *Journal of Thermophysics and Heat Transfer*, Vol. 1, No. 1, 1987, pp. 83–89.

[18]Zebib, A., Homsy, G. M., and Meiburg, E., "High Marangoni Number Convection in a Square Cavity," *Physics of Fluids*, Vol. 28, No. 12, 1985, pp. 3467–3476.

[19]Lai, C-L., Ostrach, S., and Kamotani, Y., "The Role of Free-Surface Deformation in Unsteady Thermocapillary Flow," *Heat Transfer in High Technology and Power Engineering*, edited by Wen-Jei Yang, Hemisphere, New York, 1987, pp. 15–38.

[20]Keller, J. R., and Bergman, T. L., "Thermocapillary Cavity Convection in Wetting and Nonwetting Liquids," *Numerical Heat Transfer*, Part A, Vol. 18, 1990, pp. 33–49.

[21]Abramzon, B., Edwards, D. K., and Sirignano, W. A., "Transient, Stratified, Enclosed Gas and Liquid Behavior with Concentrated Heating from Above," *Journal of Thermophysics and Heat Transfer*, Vol. 1, No. 4, 1987, pp. 355–364.

[22]Chen, M. M., "Thermocapillary Convection in Materials Processing," Hemisphere, in press.

[23]Carpenter, B. M., and Homsy, G. M., "Combined Buoyant-Thermocapillary Flow in a Cavity," *Journal of Fluid Mechanics*, Vol. 207, 1989, pp. 121–132.

[24]Chan, C. L., Chen, M. M., and Mazumder, J., "Asymptotic Solution for Thermocapillary Flow at High and Low Prandtl Numbers Due to Concentrated Surface Heating," *Journal of Heat Transfer*, Vol. 110, 1988, pp. 140–146.

[25]Patankar, S. V., *Numerical Heat Transfer and Fluid Flow*, McGraw-Hill, New York, 1980.

[26]Van Doormaal, J. P., and Raithby, G. D., "Enhancements of the SIMPLE Method for Predicting Incompressible Fluid Flows," *Numerical Heat Transfer*, Vol. 7, 1984, pp. 147–163.

[27]Schiller, D. N., Abramzon, B., and Sirignano, W. A., "Enclosed Liquid/Gas System Heated Nonuniformly From Above: Variable Properties and Vaporization Effects," 26th ASME/AIChE National Heat Transfer Conference, Philadelphia; HTD-Vol. 106, *Heat Transfer Phenomena in Radiation, Combustion, and Fires*, American Society of Mechanical Engineers, New York, NY, edited by R. K. Shah, 1989, pp. 389–398.

[28]Aggarwal, S. K., Iyengar, J., and Sirignano, W. A., "Enclosed Gas and Liquid with Nonuniform Heating from Above," *International Journal of Heat Mass Transfer*, Vol. 29, No. 10, 1986, pp. 1593–1604.

[29]Zehr, R. L., Chen, M. M., and Mazumder, J., "Thermocapillary Convection of a Differentially Heated Cavity at High Marangoni Numbers," National Heat Transfer Conference, Pittsburgh, Paper 87-HT-29, 1987.

[30]Vargaftik, N. B., *Tables on the Thermophysical Properties of Liquids and Gases*, 2nd ed., Hemisphere, Washington, DC, 1975.

[31]Touloukian, Y., *Thermophysical Properties of Matter*, Vol. 11, Plenum Press, New York, 1970.